

IFUP-TH 11/94

February 1994

hep-lat/9403016

## Field–strength correlators in SU(2) gauge theory

*L. Del Debbio, A. Di Giacomo*

Dipartimento di Fisica dell'Università and I.N.F.N.

Piazza Torricelli, 2

I-56100 Pisa, Italy

*Yu. A. Simonov*

I.T.E.P.

B.Cheremushkinskaya ulitsa 25

RU-117 259 Moskva, Russia

### Abstract

We measure field-strength and their correlators in presence of a static  $q\bar{q}$  pair by numerical simulations. We give an interpretation of these data in terms of quadratic and quartic cumulants.

# 1 Introduction

A study of the field–strength distribution between static quark and antiquark yields a detailed picture of the string formation and helps to understand the mechanism of confinement. In particular, comparing the field distributions with those of the dual Meissner model one can clarify the viability of the popular confinement mechanism.

In non-abelian theory there are two ways of measuring the field–strength distribution: using connected  $\rho^c$  or disconnected  $\rho^{disc}$  plaquette averages around the Wilson loop [1]. While both reduce to the same quantity in the Abelian case, in the non-abelian case two measurements yield independent information. Recently [1]  $\rho^c$  and  $\rho^{disc}$  have been measured for some components of the field  $F_{\mu\nu}$  using the cooling method [2]. While the signal for  $\rho^{disc}$  was too small, the distribution of  $E_{11}$  off the string axis (“the string profile”) and along the string from  $\rho^c$  was found with good accuracy. Another important quantity measured in [1] was a double plaquette correlator  $\gamma^c(x, x')$ , yielding additional information on correlation of field strength at two different points  $x, x'$  of the string.

The purpose of the present paper is: i) to extend the Monte–Carlo (MC) measurements to all orientations of the plaquettes in  $\rho^c$  and  $\gamma^c(x, x')$ , thus yielding the most complete information on the field distribution in the  $q\bar{q}$  string; ii) to give interpretation of the results in terms of simpler quantities – field strength correlators like  $\langle F_{\mu\nu}(x)F_{\rho\sigma}(y) \rangle$  (cumulants).

Using cluster expansion and non-abelian Stokes theorem [3], one can express  $\rho^c$  and  $\gamma^c$  in terms of cumulants and keep the lowest ones (physical arguments in favour of dominance of lowest cumulants are given in the review paper [4]). The latter have been recently measured on the lattice [5], yielding a rather small correlation length  $T_g = 0.2$  fm. Now, using the cumulants, one unambiguously predicts  $\rho^c$  and can compare it with MC measurements. This comparison with data from [1] was done in [6] and a good agreement of measured and calculated string profile was found. In particular it was clarified how a small correlation length  $T_g = 0.2$  fm yields a bigger radius of the string – 0.5 fm.

After presenting new measurements in sections 2 and 3, we make in section 4 a more precise and extended calculation of  $\rho^c$  in terms of the bilocal cumulant and compare it with MC data. In particular we predict vanishing of some  $\rho^c(F_{\mu\nu})$  on symmetry grounds and observe it explicitly in data. We perform the same analysis for  $\gamma^c$  and predict vanishing of most combinations of plaquette orientations. The

dominating structure  $-\gamma^c(E_{\parallel}, E_{\parallel})$  – is expressed in terms of the quartic cumulant, which has never been measured on the lattice; the data for  $\gamma^c$  allow to make some estimates of it.

A short summary of results is given in conclusion.

## 2 MC study of the field strength tensor.

Using MC technique, we study the spatial distribution of the components of the field strength tensor in presence of a  $q\bar{q}$  pair. This generalizes to all the components of the field the results already obtained in [1]. Following [1], we define:

$$\rho_{\mu\nu}^c = \frac{\langle \text{tr}(WLP_{\mu\nu}(x_{\parallel}, x_{\perp})L^+) \rangle}{\langle \text{Tr}W \rangle} - 1 \quad (1)$$

where  $W$  is a Wilson loop,  $L$  is a Schwinger line and  $P_{\mu\nu}$  is the part of the plaquette proportional to the  $\sigma$ - matrices, oriented in order to give the desired component of the field. The coordinates  $x_{\parallel}, x_{\perp}$  measure resp. the distance from the edge of the Wilson loop and from the plane defined by the loop, as shown in Fig. 1. In the naive continuum limit  $a \rightarrow 0$ ,

$$\rho_{\mu\nu}^c \simeq a^2 \langle F_{\mu\nu} \rangle_{q\bar{q}} \quad (2)$$

We have used a  $16^4$  lattice, taking a  $8 \times 8$  Wilson loop and  $\beta = 2.50$ , which is inside the scaling window for the fields. Moving the plaquette in and outside the plane defined by the Wilson loop, we obtain a map of the spatial structure of the field as a function of  $x_{\parallel}$  and  $x_{\perp}$ . Using a controlled cooling technique (see [1,2] and references therein), we eliminate the short-range fluctuations. The long-range non-perturbative effects survive longer to the cooling procedure, showing a plateau of 10–14 cooling steps, while the error becomes smaller. A similar behaviour has been observed for the string tension. The cooling technique allows us to disentangle the signal from the quantum noise with a relatively small statistics. The general patterns of the field configurations are briefly resumed in the following figures. Figure 2 represent a detailed map of the spatial behaviour of the longitudinal component of the chromoelectric field.

- Varying  $x_{\parallel}$  at fixed  $x_{\perp}$ , we investigate the structure of the fields in the direction of the axis joining the  $q\bar{q}$  pair. In Fig. 3, we show  $E_{\parallel}$  and  $B_{\perp}$  as functions of  $x_{\parallel}$  for  $x_{\perp} = 0$ , i.e. on the  $q\bar{q}$  axis. We find that the electric field remains constant and magnetic transverse field vanishes, as expected on symmetry grounds.

- Varying  $x_{\perp}$  at fixed  $x_{\parallel}$ , we study the transverse shape of the fields. Fig. 4 illustrates the behaviour of the  $E_{\parallel}$  component vs.  $x_{\perp}$ , for different values of  $x_{\parallel}$ : the field remains constant with respect to  $x_{\parallel}$  also outside the plane defined by the Wilson loop, as long as we remain inside the string (i.e. for  $x_{\parallel} = 3, 5$ ). A detailed study of the transverse shape will be given below.

We find that the parallel electric field is squeezed in flux tubes, as already found in [1]. The results in [1] were consistent with a gaussian behaviour of the flux tube profile inside the string. In order to estimate the size of our tubes and to check the consistency of the result with previous measurements, we have again performed a fit of the transverse shape inside the string (for  $x_{\parallel} = 3$ ) with the function

$$E_{\parallel} = \exp(\kappa - \mu^2 x_{\perp}^2) \quad (3)$$

finding  $\mu = 0.30 \pm 0.01$ , with  $\chi^2/\text{d.o.f.} = 0.993$ . This indicates that the flux tubes have a transverse size of the order of 3 lattice spacings at  $\beta = 2.50$ , which corresponds to a physical value  $\mu^{\text{phys}}/\Lambda_{\text{latt}} = 85 \pm 4$ , in agreement with [1]. In what follows, motivated by the measured form of the field strength correlators [5] and by the analysis in terms of cumulants [3], we will find that data are equally consistent with the form eq. (18), which is also suggested by the mechanism of confinement via dual superconductivity.

### 3 Field strength correlators

In the last years, a systematic study on non-perturbative effects in QCD in terms of the gluon field strength correlators has been developed (see Ref. [3] and references therein) and the behaviour of these correlators in the vacuum has been investigated by lattice simulations [5]. As pointed out by the authors of [3], studying the field correlators in presence of  $q\bar{q}$  pair, could provide further informations for describing color confinement. Therefore we measure the operator:

$$\gamma^c = \frac{\langle \text{Tr}\{W S V_{PP'} S^+\} \rangle}{\langle \text{Tr}W \rangle} - \langle \text{Tr}V_{PP'} \rangle \quad (4)$$

where

$$V_{PP'} = P_{\mu\nu} L P'_{\rho\sigma} L^+ - \frac{1}{2} P_{\mu\nu} \text{Tr} P'_{\rho\sigma} \quad (5)$$

where  $W$  is a Wilson loop,  $S$  is a Schwinger line connecting the Wilson loop to the  $V_{PP'}$  operator,  $P$  and  $P'$  are two plaquettes, located at  $x$  and  $x'$  respectively, and  $L$  is a Schwinger line connecting them.

In the naive continuum limit, we have

$$\gamma^c = a^2 \langle F' \rangle + a^4 [\langle FF' \rangle_{q\bar{q}} - \langle FF' \rangle_0] \quad (6)$$

where  $F$  and  $F'$  are respectively the field components at  $x$  and  $x'$ .

Varying the orientations of the two plaquettes, we obtain the different components of the correlators. The measurements have been done on a  $12^4$  lattice at  $\beta = 2.50$  using  $6 \times 6$  Wilson loop. Again, we used controlled cooling to reduce the fluctuations. We have measured  $\gamma^c$  with the following two types of orientations of  $F$  and  $F'$ .

(i) In the first case:

- $P$  is held fixed on the  $q\bar{q}$  axis at 1 lattice spacing from the border of the Wilson loop, while its orientation is varied in the 6 possible directions;
- $P'$  is moved in- and outside the plane of the Wilson loop, its orientation is kept fixed in the  $E_{\parallel}$  direction;
- $x_{\parallel}$  and  $x_{\perp}$  identify the position of  $P'$  with respect to  $P$ .

(ii) In the second type of measurements:

- both the position and the orientation of  $P$  are kept fixed; the plaquette is in the same position as before and its orientation corresponds to the  $E_{\parallel}$  component;
- $P'$  is moved as before and its orientation is changed.

We finally define the irreducible correlator  $\bar{\gamma}^c$  as follows

$$\bar{\gamma}^c \equiv \gamma^c(x, x') - \rho^c(x') \approx a^4 [\langle FF' \rangle_{q\bar{q}} - \langle FF' \rangle_0] \quad (7)$$

From (7) it is clear, that  $\bar{\gamma}^c$  contains only double plaquette correlations.

Most of the data for  $\gamma^c$  and  $\bar{\gamma}^c$  are compatible with zero net effect, within two standard deviations. In Table 1, we report the data for  $\bar{\gamma}^c$  in case when both plaquettes  $P$  and  $P'$  are kept fixed in the  $E_{\parallel}$  direction. In the next Section we compare the Monte–Carlo measurements with the predictions from the cumulant (cluster) expansion and will see that indeed all orientations except  $E_{\parallel}, E_{\parallel}$  should give zero result due to simple symmetry arguments.

## 4 Extracting bilocal and quartic field-strength correlators from the Monte–Carlo data

For the contour  $C$  shown in Fig. 1 we denote direction along the  $q\bar{q}$  axis  $x_{\parallel} = x_1$ , while that of  $x_{\perp} = x_2$ , and the Euclidean temporal axis is  $x_4$ . All the construction in Fig. 1 is taken at a fixed value of  $x_3$ .

Using the non-abelian Stokes theorem and the cluster expansion [3] for  $\rho_{\mu\nu}^c$  in (1) one has (see [6] for details of derivation)

$$\rho_{\mu\nu}^c(x_1, x_2, x_4) = a^2 \int d\sigma_{14}(x'_1, x'_4) \Lambda_{\mu\nu} \quad (8)$$

where

$$\Lambda_{\mu\nu} = \frac{1}{N_c} \text{tr} \langle E_1(x'_1, 0, x'_4) \Phi F_{\mu\nu}(x_1, x_2, x_4) \Phi^+ \rangle + \dots, \quad (9)$$

$\Phi$  is the parallel transporter (Schwinger line) from the point  $(x'_1, 0, x'_4)$  to  $(x_1, x_2, x_4)$ , and dots imply contribution of higher order cumulants, containing additional powers of  $E_1$  [3].

We shall keep throughout this Section only the lowest cumulants (containing lowest power of  $E_1$ ) and compare our prediction with the MC data of previous sections. The bilocal correlator  $\Lambda_{\mu\nu}$  can be expressed in terms of two independent Lorentz scalar functions  $D((x_\mu - x'_\mu)^2)$ ,  $D_1((x_\mu - x'_\mu)^2)$  (see [3] and the appendix 1 of the last ref. in [3])

$$\Lambda_{14} = D + D_1 + (h_1^2 + h_4^2) \frac{dD_1}{dh^2} \quad (10)$$

$$\Lambda_{24} = (h_1 h_2) \frac{dD_1}{dh^2}, \quad \Lambda_{34} = (h_1 h_3) \frac{dD_1}{dh^2} \quad (11)$$

$$\Lambda_{23} \equiv 0, \quad \Lambda_{13} = h_3 h_4 \frac{dD_1}{dh^2}; \quad \Lambda_{12} = h_2 h_4 \frac{dD_1}{dh^2} \quad (12)$$

Here  $h_\mu = (x - x')_\mu$ .

Since all construction in Fig. 1 is at  $x_3 = x'_3 = 0$  we have  $h_3 \equiv 0$  and hence

$$\rho_{23}^c = \rho_{34}^c = \rho_{13}^c \equiv 0 \quad (13)$$

The only nonzero components are  $\Lambda_{14}$ ,  $\Lambda_{24}$  and  $\Lambda_{12}$ . For the latter the contribution to  $\rho^c$  can be written as

$$\rho_{12}^c(x_1, x_2, x_4) = a^2 \int_0^R dx'_1 \int_{-\frac{T}{2}}^{\frac{T}{2}} dx'_4 (+x_2)(x_4 - x'_4) \frac{dD_1(h^2)}{dh^2} \quad (14)$$

When  $x_4 = 0$  (and this is where measurements of  $\rho_{12}^c$  have been done),  $\rho_{12}^c$  vanishes because of antisymmetry of the integrand in (14).

Hence only  $\rho_{14}^c$  and  $\rho_{24}^c$  are nonzero, and only those have been measured to be nonzero.

To make comparison with data more quantitative, let us exploit recent MC calculation of  $D$  and  $D_1$  [5], which imply that both  $D$  and  $D_1$  are of exponential form

$$D_1(h^2) = D_1(0) \exp(-\mu_1 h); \quad D(h^2) = D(0) \exp(-\mu h) \quad (15)$$

$$D_1(0) \approx \frac{1}{3}D(0); \quad \mu_1 \approx \mu$$

Inserting this into (8), (14) we have

$$\rho_{14}^c(x_1, x_2; 0) = a^2 \int_0^R dx'_1 \int_{-\frac{T}{2}}^{\frac{T}{2}} dx'_4 [D(0) + D_1(0) - \frac{(h_4^2 + h_1^2)}{2h} D_1(0)] e^{-\mu h} \quad (16)$$

with

$$h_4 = -x'_4, \quad h_1 = x_1 - x'_1, \quad h^2 = h_4^2 + h_1^2 + x_2^2;$$

For  $\rho_{24}^c$  similarly one obtains

$$\rho_{24}^c(x_1, x_2; 0) = -a^2 \mu x_2 \int_0^R dx'_1 \int_{-\frac{T}{2}}^{\frac{T}{2}} dx'_4 \frac{(x_1 - x'_1)}{2h} D_1(0) e^{-\mu h} \quad (17)$$

From (16) and (17) one can deduce, that

- (i)  $\rho_{24}^c$  should vanish for  $x_2 = 0$
- (ii)  $\rho_{24}^c$  changes sign for  $x_1 = \frac{R}{2}$ , i.e. in the middle of the string length.
- (iii)  $\rho_{24}^c$  is about 1/3 of  $\rho_{14}^c$ .

All properties (i)–(iii) are supported by the data.

Finally, we can make a detailed comparison of our prediction for  $\rho_{14}^c$  in (16) with data. One obtains a simple analytic result for  $\rho_{14}^c(x_2 \equiv x_\perp)$  in case of a very long string. The transverse shape measured at the middle is given by [6]

$$\rho_{14}^c = \frac{2\pi a^2}{\mu^2} [D(0)(1 + \mu x_2) - D_1(0) \frac{1}{2} (\mu x_2)^2] e^{-\mu x_2} \quad (18)$$

As shown in [6], this shape is in good agreement with the previous data, obtained in [5]. Here we calculate  $\rho_{14}^c$  as a function of  $x_1, x_2$  from (16) keeping  $D_1(0) = \frac{1}{3}D(0)$ . We then fit the data for  $x_\parallel = 3$  to evaluate  $\mu$  and  $a^2 D(0)$ . We find:

$$\mu \approx 0.19 \text{ fm}, \quad a^2 D(0) \approx 3.92 \times 10^7$$

with a  $\chi^2/\text{d.o.f} = 0.17$ .

The value of  $\mu$  is in good agreement with [5], while we find that  $a^2 D(0)$  is one order of magnitude smaller than in the previous measurements. We recall that our data here are obtained for  $SU(2)$ , while in [5] the gauge group was  $SU(3)$ . This should account for the one order of magnitude between the two results.

These results allow to predict all curves for other values of  $x_\parallel$  and  $x_\perp$ : the agreement with the numerical results is very satisfactory as can be seen from Fig. 4.

We turn now to the double correlator  $\bar{\gamma}_{\mu\nu}^c$ , Eq. (7). We again use the non-abelian Stokes theorem and the cluster expansion, to represent  $\bar{\gamma}^c$  as

$$\begin{aligned} \bar{\gamma}_{\mu\nu,\mu'\nu'}^c(x,x') &= \frac{a^4}{4!} \int dy_1 dy_4 du_1 du_4 \{ \ll E_1(y) \Phi E_1(u) \Phi F_{\mu\nu}(x) \times \\ &\quad \Phi F_{\mu'\nu'}(x') \Phi \gg + perm \} \\ &+ a^4 \frac{(-i)}{3!} \int dy_1 dy_4 \{ \ll E_1(y) \Phi F_{\mu\nu}(x) \Phi F_{\mu'\nu'}(x') \Phi \gg + perm \} \end{aligned} \quad (19)$$

where the sum is over permutations of the order in which  $E_1$  and  $F_{\mu\nu}$  appear under the sign of the cumulant; the latter is denoted by double angular brackets and implies that vacuum insertions are subtracted from the averages of the field strengths.

In our MC calculations partly reported in Table 2, the orientation of the plaquette  $P$  or  $P'$  was kept along the plane 14, and we should consider accordingly in (19) always  $E_1(x)$  or  $E_1(x')$  inside the cumulants.

Now the symmetry requirements impose severe conditions on the nonzero values of  $\bar{\gamma}_{\mu\nu,\mu'\nu'}^c$ . Since both  $P$  and  $P'$  are chosen in the middle of the  $x_4$  interval for the Wilson loop  $[-\frac{T}{2}, \frac{T}{2}]$ , one can use the symmetry with respect to the change  $x_4 \rightarrow -x_4$ . In this way one can show that all odd-power averages of the type  $\ll E_1(u) \Phi E_1(y) \Phi \dots E_1(P') \Phi \gg$  should vanish, since they are odd with respect to  $x_4 \rightarrow -x_4$ .

This property holds if one inserts in this odd-power cumulant additionally several magnetic field operators  $B_i, B_k \dots$

Similarly, the correlator containing  $B_i(P)$  should depend on , e.g.

$$\ll E_1(u) \Phi B_i(x) \Phi E_1(x') \Phi \gg \sim e_{ikl} h_k h_l \quad (20)$$

and therefore should vanish whenever  $h_k$  or  $h_l$  are zero for both intervals, with  $h_\mu = (u-x)_\mu$ ,  $h'_\mu = (u-x')_\mu$ . In this way one proves that (20) vanishes for  $i = 1$  or 2 identically, since  $h_3 = h'_3 \equiv 0$ . For  $i = 3$  the combination (20) should vanish when  $h_2 = h'_2 = 0$ . Using those criteria we keep in our Table 1 only results for  $\gamma_{14,14}$ , where the signal is largest. The contribution to  $\gamma_{14,14}$  comes only from the quartic cumulants in (19), since as we discussed above, the triple correlator  $\ll E, \Phi E_1 \Phi E_1 \Phi \gg$  vanishes identically .

One can conclude from the Table 1, that the quartic cumulant sharply decreases for large  $x_\perp$ , and the transverse shape of the string, using  $\bar{\gamma}_c$ , is similar to that deduced from  $\rho_c$ , the thickness of the string being of the order of 3 lattice spacings.

All the correlations  $\gamma_{\mu\nu,\mu'\nu'}$ , which should vanish on symmetry grounds, have been found to be zero within two standard deviations. In these cases, a higher statistics should be necessary for a clear answer.

## 5 Conclusions

One should stress three different aspects of the results reported above. First of all, we have presented the most detailed measurements of the connected correlators made so far. There is an agreement between the field distributions of this paper and those reported in [1], where only correlators of  $E_{11}$  were measured to be nonzero. Here with better statistics all components of magnetic field  $\vec{B}$  and electric field  $\vec{E}$  are given for all possible configurations of one probing plaquette (for  $\rho_c$ ) and two probing plaquettes (for  $\bar{\gamma}^c$ ). Symmetry requirements impose severe restrictions on  $\rho_c$  and  $\bar{\gamma}^c$  (independently on cluster expansion) and predict zero results in most cases, except for  $E_{11}(\rho_{14}^c)$ ,  $E_2(\rho_{24}^c)$  and for  $\bar{\gamma}^c(E_{11}, E_{11})$ . Results are compatible with the predictions, and hence statistical errors seem to be reliable.

Secondly, our results serve to check the validity and usefulness of the cluster expansion for the signals like  $\rho^c$ ,  $\bar{\gamma}^c$ . This expansion allows to express  $\rho^c$  and  $\bar{\gamma}^c$  in terms of a simpler (and more fundamental) bilocal correlator  $G_2 \equiv \langle F\Phi F\Phi \rangle$ , which has been measured earlier [5] and thus yields a clear prediction for  $\rho^c$  and  $\bar{\gamma}^c$ . Comparison with measured results made earlier in [6] and here in more detail in Fig. 3,4, shows a good agreement and supports the fundamentality of the bilocal correlator, which is known to define the nonperturbative dynamics of confinement [3].

In particular the asymptotics of the string profile at large  $x_\perp$  is shown to be exponential, see eq. (18), just as the asymptotics of  $G_2$ , measured in [5]. This in contrast to the behaviour inside the string, where the Gaussian-like flattening is observed before [1] and also in this paper. This effect is connected to the flattening of  $G_2(x)$  at small  $x$ , necessary for its regularity at  $x = 0$  (Note that the latter property of  $G_2$  was not taken into account in (15)) and also because of the smearing effect due to integration in (16), yielding polynomial factors in (18).

Of special importance is the first estimate of quartic cumulant  $G_4 \equiv \langle (F\Phi)^4 \rangle$  through  $\bar{\gamma}^c$  in (19).

To obtain a more quantitative measure of  $G_4$ , we represent the coordinate dependence of  $G_4$  as an exponent similarly to  $G_2$  (15) with the same  $\mu$ . In this case the

dimensionless ratio is

$$\frac{G_4(0)}{(G_2(0))^2} = \frac{\bar{\gamma}^c(0)}{\rho^c(0)^2} \approx 2 - 3$$

This kind of estimate would result from the instanton-type vacuum with instantons of small size  $\rho, \rho \leq 0.3 fm$  and typical density of one instanton per  $fm^4$  [7].

Finally, let us compare the transverse shape of the string (the string profile) measured in Table 1 and analytically written in (18) with that of the dual Meissner effect. As is known from the theory of the type-II superconductors [8, Eq.(48.11)] the asymptotics of the magnetic field distribution off the vortex line is exponential,  $B(r) \sim exp(-r/\delta)$ , where  $\delta$  is the so-called London's penetration length. One can see that the dual Meissner effect is capable of reproducing such fine details of the confinement picture, as the field distribution around the string.

This conclusion agrees with a recent study made in a completely different approach in [9].

### **Acknowledgements**

This work has been started, when one of the authors (Yu.S.) was visiting Department of Physics of Pisa University. It is a pleasure for him to thank the Department for a kind hospitality, and to acknowledge a financial support of the Russian Fund for Fundamental Research. LDD wants to thank the Italian ALEPH group at CERN for the warm hospitality during the final part of this work.

## References

- [1] A. Di Giacomo, M. Maggiore and S. Olejnik, Phys. Lett. **236 B**(1990) 199; Nucl. Phys. **B347** (1990) 441.
- [2] M. Campostrini et al., Phys. Lett. **225B** (1989) 403.
- [3] H. G. Dosch, Phys. Lett. **190B** (1987) 177;  
H. G. Dosch & Yu. A. Simonov, Phys. Lett. **205B** (1988) 339;  
Yu. A. Simonov, Nucl. Phys. **B234** (1989) 67.
- [4] Yu. A. Simonov, Yad. Fiz. **54** (1991) 192.
- [5] M. Campostrini, A. Di Giacomo and G. Mussardo, Z. Phys. C 25 (1984) 173;  
A. Di Giacomo & H. Panagopoulos, Phys. Lett. **285B** (1992) 133.
- [6] Yu. A. Simonov, What the QCD string is made of, Preprint ITEP 28-92 (unpublished).
- [7] M. A. Shifman, A. I. Vainshtein and V. I. Zakharov, Nucl. Phys. B147 (1979) 385.
- [8] E. M. Lifshitz and L. P. Pitaevski, Statistical Physics, part 2, Theory of Condensed Matter, chapter 47.
- [9] V. Singh, D. A. Browne and R. W. Haymaker, Phys. Lett. **B306** (1993)115.

## Figure Caption

- Figure 1: The operator  $\rho^c$ .
- Figure 2: The spatial structure of the parallel chromoelectric field  $E_{\parallel}$ .
- Figure 3: Different components of the field–strength tensor ( $E_{\parallel}$  and  $B_{\parallel}$ , circles and diamonds respectively) vs.  $x_{\parallel}$  at fixed  $x_{\perp} = 0$ .
- Figure 4:  $E_{\parallel}$  vs.  $x_{\perp}$ , for  $x_{\parallel} = 1, 3, 5, 7$  (triangles up, filled circles, diamonds and triangles down resp.). The dashed and solid lines are the results of the fits performed using resp. formula (18) and (3).

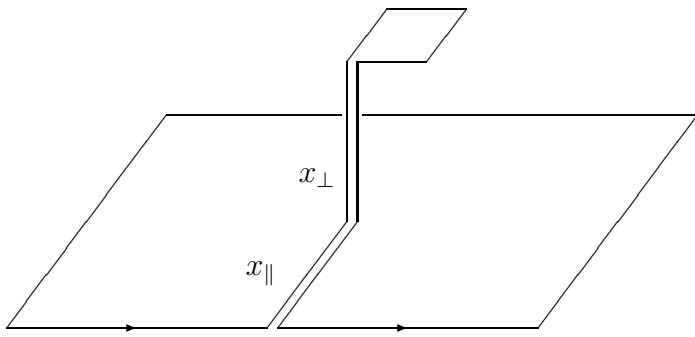


Figure 1: The operator  $\rho^c$ .

Figure 2: Spatial distribution of  $E_{\parallel}$

Figure 3:  $E_{\parallel}, B_{\parallel}$  vs.  $x_{\parallel}$ , for  $x_{\perp} = 0$ .

Figure 4:  $E_{\parallel}$  vs.  $x_{\perp}$ .

$x_{\perp}$	$E_{\parallel}$
0	$-.032893 \pm 0.008056$
1	$-.029240 \pm 0.006531$
2	$-.020212 \pm 0.005298$
3	$-.010907 \pm 0.004644$
4	$-.005311 \pm 0.004136$
5	$-.001269 \pm 0.004222$
6	$0.000397 \pm 0.003870$

Table 1:  $\bar{\gamma}^c$  vs.  $x_{\perp}$ ,  $x_{\parallel} = 1$ .

This figure "fig1-1.png" is available in "png" format from:

<http://arxiv.org/ps/hep-lat/9403016v1>

This figure "fig1-2.png" is available in "png" format from:

<http://arxiv.org/ps/hep-lat/9403016v1>

This figure "fig1-3.png" is available in "png" format from:

<http://arxiv.org/ps/hep-lat/9403016v1>